

REPORTS

NONLINEAR OPTICS

Large optical nonlinearity of indium tin oxide in its epsilon-near-zero region

M. Zahirul Alam,¹ Israel De Leon,^{1,3*} Robert W. Boyd^{1,2}

Nonlinear optical phenomena are crucial for a broad range of applications, such as microscopy, all-optical data processing, and quantum information. However, materials usually exhibit a weak optical nonlinearity even under intense coherent illumination. We report that indium tin oxide can acquire an ultrafast and large intensity-dependent refractive index in the region of the spectrum where the real part of its permittivity vanishes. We observe a change in the real part of the refractive index of 0.72 ± 0.025 , corresponding to 170% of the linear refractive index. This change in refractive index is reversible with a recovery time of about 360 femtoseconds. Our results offer the possibility of designing material structures with large ultrafast nonlinearity for applications in nanophotonics.

A long-standing goal in nonlinear optics has been the development of materials whose refractive index can be drastically changed using a low-power optical field. Ideally, these materials should possess subpicosecond time response and be compatible with existing complementary metal-oxide semiconductor (CMOS) fabrication technologies (1–2). Simple calculus shows that, for a given change ($\Delta\epsilon$) in the permittivity ϵ , the resulting change (Δn) in the refractive index n is given for a lossless material by $\Delta n = \Delta\epsilon / (2\sqrt{\epsilon})$. We see that this change becomes large as the permittivity becomes small, suggesting that the epsilon-near-zero (ENZ) frequencies of a material system should give rise to strong nonlinear optical properties.

Materials possessing free charges, such as metals and highly doped semiconductors, have zero real permittivity at the bulk plasmon wavelength. A number of authors have reported on the unusual properties of matter under ENZ conditions (3–5) and on their promise for applications in nonlinear optics (6–10).

We used commercially available indium tin oxide (ITO), a CMOS-compatible degenerate semiconductor, as the ENZ medium (Fig. 1). The zero-permittivity wavelength of ITO occurs at near-infrared wavelengths and can be tuned by controlling the doping density or by applying a static electric field (11, 12). The z -scan technique was used to characterize the intensity-dependent refractive index of ITO for transverse magnetic (TM) polarized light (Fig. 2A) (13, 14). The wavelength-dependent effective nonlinear refractive index coefficient $n_{2(\text{eff})} = \Delta n / I$ (I is the intensity of the laser

beam) and effective nonlinear attenuation constant $\beta_{(\text{eff})} = \Delta\alpha / I$ extracted from our measurements are plotted for angles of incidence varying from $\theta = 0^\circ$ to $\theta = 60^\circ$ (Fig. 2, A and B). The results indicate that ITO exhibits positive $n_{2(\text{eff})}$ and negative $\beta_{(\text{eff})}$, corresponding to self-focusing and saturable absorption, respectively. Our results reveal a substantial wavelength- and angle-dependent enhancement of the material's nonlinear response at ENZ wavelengths. The measured value of $n_{2(\text{eff})}$ ($6 \times 10^{-5} \text{ cm}^2/\text{GW}$) at the shortest wavelength (970 nm) agrees well with the value reported by Elim *et al.* (15). At a wavelength of 1240 nm for normal incidence, $n_{2(\text{eff})}$ and $\beta_{(\text{eff})}$ are ~ 43 and ~ 53 times larger than the corresponding values at 970 nm, respectively. For TM-polarized light at oblique incidence, the nonlinear response is further enhanced. The enhancement factors, defined relative to the values far from the ENZ spectral region (at $\lambda = 970$ nm) at normal incidence, are plotted as functions of θ in Fig. 2C. The enhancement tends to increase with θ for $0^\circ < \theta < 60^\circ$ and decreases sharply for $\theta > 60^\circ$. The maximum enhancement factors, measured at $\theta = 60^\circ$, are 1837 and 2377 for $n_{2(\text{eff})}$ and $\beta_{(\text{eff})}$, respectively. Thus, at $\lambda_0 = 1240$ nm, the $n_{2(\text{eff})}$ and $\beta_{(\text{eff})}$ values

for $\theta = 60^\circ$ are ~ 43 and ~ 45 times larger than for normal incidence, respectively.

The temporal dynamics of the optical nonlinear response was studied using a degenerate pump-probe transmission measurement. Here, an intense pump pulse and a weak probe pulse at the same wavelength interact with the sample, and the induced change in probe transmittance ΔT is measured as a function to the time delay τ between the two pulses. The measured temporal response is proportional to the convolution of the probe's temporal envelope with the material's temporal response function. (Fig. 2D). The transient nonlinear response has a rise time no longer than 200 fs (this estimate is limited by our laser pulse duration) and a recovery time of 360 fs. Such ultrafast response would allow all-optical modulation speeds of at least 1.5 THz.

The nonlinear coefficients shown in Fig. 2, A and B, may be slightly overestimated because the z -scan method neglects the change in reflectivity caused by Δn (16), but this overestimation is no larger than by a factor of ~ 1.8 . In any case, the measured values are extremely large. In particular, the value of $n_{2(\text{eff})} = 0.11 \text{ cm}^2/\text{GW}$ measured at $\theta = 60^\circ$ is more than two orders of magnitude larger than that of As_2Se_3 chalcogenide glass (17) and ~ 5 times larger in magnitude than that of a recently proposed highly nonlinear metamaterial (6). The optical losses of ITO at ENZ wavelengths can be quite large, although in (16) we describe some realistic applications that can tolerate this much loss.

We attribute the observed nonlinearity primarily to a modification of the energy distribution of conduction-band electrons as a consequence of the laser-induced electron heating. We describe the nonlinear optical response by means of a phenomenological two-temperature model (16, 18–20). Figure 3A shows the calculated temporal evolution of the free-electron temperature (T_e) and lattice temperature (T_l) of ITO after irradiation by the laser pulse (denoted by the dashed curve). The free-electron temperature exhibits an ultrafast transient and is limited by the electron-phonon relaxation time of the material (21). The normalized transient nonlinear response measured via the degenerate pump-probe technique is well described by the temporal profiles of T_e convolved with the probe's intensity envelope, which is plotted as the solid curve in Fig. 2D.

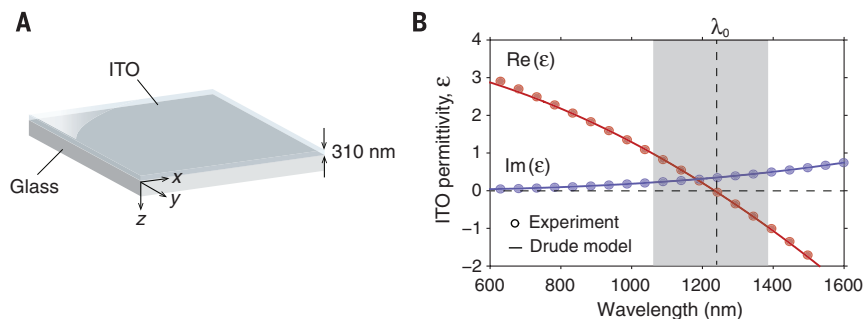


Fig. 1. The ITO sample under investigation and its linear optical response. (A) Structure under investigation. (B) Linear relative permittivity of the ITO film measured via spectroscopic ellipsometry (symbols) and estimated by the Drude model (lines). The condition $\text{Re}(\epsilon) = 0$ occurs at $\lambda_0 = 1240$ nm. The shaded region shows the spectral range investigated in our nonlinear optical characterization.

¹Department of Physics and Max Planck Centre for Extreme and Quantum Photonics, University of Ottawa, 25 Templeton Street, Ottawa, ON, K1N 6N5, Canada. ²Institute of Optics and Department of Physics and Astronomy, University of Rochester, Rochester, NY 14627, USA. ³School of Engineering and Sciences, Tecnológico de Monterrey, Monterrey, Nuevo León 64849, Mexico.

*Corresponding author. Email: ideleon@itesm.mx

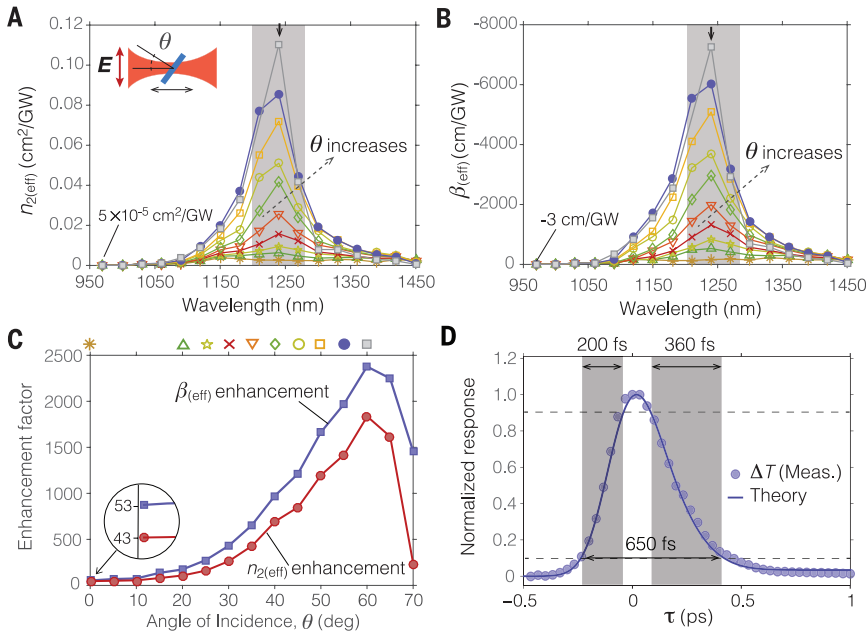


Fig. 2. Nonlinear optical response of the ITO sample. Wavelength dependence of (A) the nonlinear effective refractive index, $n_{2(\text{eff})}$, and (B) the effective nonlinear attenuation constant, $\beta_{(\text{eff})}$. The nonlinear response is enhanced in the ENZ region of the spectrum (shaded). The vertical arrows indicate the wavelength $\lambda_0 = 1240$ nm. (C) The corresponding enhancement for $n_{2(\text{eff})}$ and $\beta_{(\text{eff})}$ at λ_0 , compared with values at 970 nm, are plotted as functions of θ . The values of θ corresponding to the different symbols in (A) and (B) are indicated at the top. (D) Time dependence of the normalized transient change of transmittance (ΔT) obtained via a degenerate pump-probe measurement.

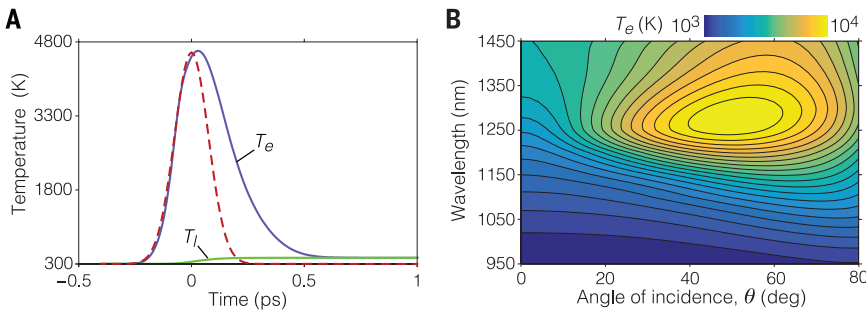


Fig. 3. Numerical modeling of the hot-electron dynamics of ITO. (A) Transient response of T_e and T_l obtained using the two-temperature model. The dashed curve denotes the pulse intensity profile (in arbitrary units). (B) Map of the peak free-electron temperature in ITO calculated as a function of θ and λ . Both calculations assume a normally incident laser with an intensity of 66 GW/cm^2 .

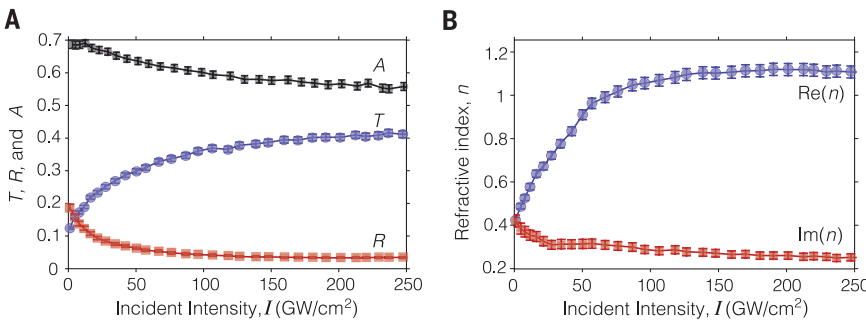


Fig. 4. Nonlinear optical response of ITO for laser fields sufficiently intense to produce saturation. (A) Intensity-dependent transmittance (T), reflectance (R), and absorptance (A) of the ITO-glass structure at λ_0 for $\theta = 30^\circ$. (B) Complex effective refractive index of ITO extracted from the measured values in (A) using a transfer-matrix method.

The peak values of T_e obtained with our model are plotted in Fig. 3B as functions of the wavelength and the angle of incidence. The temperature profile exhibits the main features present in our experimental results, namely a pronounced enhancement of the response at ENZ wavelengths that reaches a maximum for an angle of incidence close to $\theta = 60^\circ$. The general behavior observed in this result can be understood in terms of two contributions. The increasing values of T_e for longer wavelengths result from the increase in free carrier absorption, and the peak that develops around $\theta \approx 60^\circ$ results from an enhancement of the electric field within the ITO film. This enhancement occurs only for obliquely incident TM polarized light at wavelengths within the ENZ region and follows from the continuity of the normal electric displacement field across an ITO-air interface (16, 22). As discussed in (16), $\Delta\epsilon$ results from an effective red shift in the material's plasma frequency caused by an increase in the free-electron temperature (ΔT_e). It is important to note that $\Delta\epsilon$ does not scale linearly with ΔT_e for a large ΔT_e and that Δn is a nonlinear function of $\Delta\epsilon$ at ENZ. Consequently, a modest field intensity enhancement in the ITO film can lead to a large enhancement of $n_{2(\text{eff})}$ at ENZ wavelengths. This is confirmed by our model presented in (16), which accounts for such nonlinear relationships between Δn , $\Delta\epsilon$, and ΔT_e .

The hot-electron-induced optical nonlinearity of ITO at ENZ wavelengths differs from that of noble metals under infrared irradiation in two ways. First, as argued above, for a given change in permittivity, the nonlinear change in refractive index is always larger in the ENZ region than in non-ENZ regions. Second, the free-electron heat capacity of ITO ($4.53 \text{ Jm}^{-3}\text{K}^{-1}$) is more than an order of magnitude smaller than that of a noble metal such as gold. Thus, the increase in the free-electron temperature compared with the Fermi temperature and the consequent change in refractive index in ITO is much larger.

For sufficiently large optical intensities, the nonlinear response of ITO at ENZ wavelengths can lead to changes in its refractive index that are larger than the linear refractive index. As a result, the Fresnel reflection and transmission coefficients undergo a large change as a function of the incident optical intensity. To demonstrate this phenomenon, we measured the intensity-dependent transmittance (T), reflectance (R), and absorptance (A) of the sample at 1240 nm for $\theta = 30^\circ$ (Fig. 4A). At the lowest intensity, these measurements agree well with the predictions of a simple linear Fresnel analysis. As the intensity is increased, we observe a large monotonic increase (reduction) in transmittance (reflectance). The maximum reduction in absorptance is $\sim 30\%$, which is consistent with the saturable absorption observed in our z -scan measurements. The real part of the refractive index of ITO undergoes a dramatic change from its linear value of 0.42 to a value of 1.14 ± 0.025 for an intensity of 150 GW/cm^2 (Fig. 4B). Similarly, the imaginary part of the index is substantially reduced from

its linear value of 0.42 to a value of 0.27 ± 0.015 at this intensity. Both the real and the imaginary parts of the refractive index saturate for even higher input power. We found that these measurements are highly repeatable and that the material does not exhibit a permanent change of its optical properties.

The magnitude of the optically induced ultrafast change of the real part of the refractive index ($\Delta n = 0.72 \pm 0.025$) and the relative change of 170% in comparison to the linear value are unprecedented. The change in the refractive index corresponds to a change of the permittivity from $\epsilon = 0 + 0.352i$ to $\epsilon = 1.22 + 0.61i$ where i is the square root of -1 . This result shows that ITO can exhibit a reversible transition from metallic to a lossy dielectric state with a subpicosecond time response at wavelengths slightly longer than the bulk plasmon wavelength. Moreover, the usual perturbation expansion description of nonlinear optical effects is not applicable for this material at high intensities.

We have shown that a thin ITO film exhibits an extremely large ultrafast third-order nonlinearity at ENZ wavelengths. Moreover, it can acquire an optically induced change in the refractive index that is unprecedentedly large. Our results challenge the notion that the nonlinear optical response is only a perturbation to the linear response. Materials with such a large nonlinear response are expected to enable exotic nonlinear dynamics (22) and allow all-optical control of metasurface and active plasmonics devices. Thus, our results introduce a completely new paradigm in nonlinear optics and open new avenues for developing optical nanostructures with large nonlinearity for applications in nanophotonics, plasmonics, and nonlinear nano-optics.

REFERENCES AND NOTES

- M. Kauranen, A. V. Zayats, *Nat. Photonics* **6**, 737–748 (2012).
- M. Abb, P. Albella, J. Aizpurua, O. L. Muskens, *Nano Lett.* **11**, 2457–2463 (2011).
- M. Silveirinha, N. Engheta, *Phys. Rev. Lett.* **97**, 157403 (2006).
- A. Altu, M. Silveirinha, A. Salandrino, N. Engheta, *Phys. Rev. B* **75**, 155410 (2007).
- A. R. Davoyan, A. M. Mahmoud, N. Engheta, *Opt. Express* **21**, 3279–3286 (2013).
- A. D. Neira et al., *Nat. Commun.* **6**, 7757 (2015).
- H. Suchowski et al., *Science* **342**, 1223–1226 (2013).
- A. Capretti, Y. Wang, N. Engheta, L. Dal Negro, *Opt. Lett.* **40**, 1500–1503 (2015).
- T. S. Luk et al., *Appl. Phys. Lett.* **106**, 151103 (2015).
- N. Kinsey et al., *Optica* **2**, 616 (2015).
- G. V. Naik, V. M. Shalaev, A. Boltasseva, *Adv. Mater.* **25**, 3264–3294 (2013).
- E. Feigenbaum, K. Diest, H. A. Atwater, *Nano Lett.* **10**, 2111–2116 (2010).
- M. Sheik-Bahae, A. A. Said, T.-H. Wei, D. J. Hagan, E. W. Van Stryland, *IEEE J. Quantum Electron.* **26**, 760–769 (1990).
- B. K. Rhee, J. S. Byun, E. W. Van Stryland, *J. Opt. Soc. Am. B* **13**, 2720 (1996).
- H. I. Elim, W. Ji, F. Zhu, *Appl. Phys. B* **82**, 439–442 (2006).
- See supplementary materials on Science Online.
- R. W. Boyd, *Nonlinear Optics* (Elsevier, 2008).
- C. Sun, F. Vallée, L. Aciofi, E. P. Ippen, J. G. Fujimoto, *Phys. Rev. B Condens. Matter* **48**, 12365–12368 (1993).
- S. D. Brorson, J. G. Fujimoto, E. P. Ippen, *Phys. Rev. Lett.* **59**, 1962–1965 (1987).
- E. Carpene, *Phys. Rev. B* **74**, 024301 (2006).
- B. Rethfeld, A. Kaiser, M. Vicanek, G. Simon, *Phys. Rev. B* **65**, 214303 (2002).
- D. de Ceglia, S. Campione, M. A. Vincenti, F. Capolino, M. Scalora, *Phys. Rev. B* **87**, 155140 (2013).

ACKNOWLEDGMENTS

The authors gratefully acknowledge the support of the Canada Excellence Research Chairs Program. R.W.B. is the cofounder and Chief Technology Officer of KBN Optics, Pittsford, NY.

SUPPLEMENTARY MATERIALS

www.sciencemag.org/content/352/6287/795/suppl/DC1
Materials and Methods
Supplementary Text
Figs. S1 to S4
References (23–32)

7 December 2015; accepted 12 April 2016
Published online 28 April 2016
10.1126/science.aae0330

CATALYSIS

Photochemical route for synthesizing atomically dispersed palladium catalysts

Pengxin Liu,¹ Yun Zhao,¹ Ruixuan Qin,¹ Shiguang Mo,¹ Guangxu Chen,¹ Lin Gu,² Daniel M. Chevrier,³ Peng Zhang,³ Qing Guo,¹ Dandan Zang,¹ Binghui Wu,¹ Gang Fu,^{1*} Nanfeng Zheng^{1*}

Atomically dispersed noble metal catalysts often exhibit high catalytic performances, but the metal loading density must be kept low (usually below 0.5%) to avoid the formation of metal nanoparticles through sintering. We report a photochemical strategy to fabricate a stable atomically dispersed palladium–titanium oxide catalyst (Pd_1/TiO_2) on ethylene glycolate (EG)–stabilized ultrathin TiO_2 nanosheets containing Pd up to 1.5%. The Pd_1/TiO_2 catalyst exhibited high catalytic activity in hydrogenation of C=C bonds, exceeding that of surface Pd atoms on commercial Pd catalysts by a factor of 9. No decay in the activity was observed for 20 cycles. More important, the Pd_1/TiO_2 -EG system could activate H_2 in a heterolytic pathway, leading to a catalytic enhancement in hydrogenation of aldehydes by a factor of more than 55.

Atomically dispersed catalysts with mononuclear metal complexes or single metal atoms anchored on supports have recently attracted increasing research attention (1–15). With 100% metal dispersity, atomically dispersed catalysts offer the maximum atom efficiency, providing the most ideal strategy to create cost-effective catalysts, particularly those based on Earth-scarce metals such as Pt (1–5), Au (5–8), Pd (9–12), and Ir (13, 14). Moreover, the uniform active sites of atomically dispersed catalysts make them a model system to understand heterogeneous catalysis at the molecular level (4, 6, 10, 12–14, 16–21), bridging the gap between heterogeneous and homogeneous catalysis.

During the past decade, several strategies for atomically dispersing metal sites on catalyst supports have emerged; these include lower-

ing the loading amount of metal components (1, 8–10, 12, 20), enhancing the metal-support interactions (4, 6, 9, 19), and using voids in supports or vacancy defects on supports (3, 11, 14, 22). In most cases, the supports for atomically dispersed catalysts are deliberately chosen. Zeolites provide effective voids to anchor individual metal atoms therein and prevent them from sintering during catalysis (23, 24). Defects on reducible oxides (e.g., TiO_2 and CeO_2) (25, 26) and on graphene or C_3N_4 (9, 11, 22) help to stabilize atomically dispersed metal atoms on supports. Coordinatively unsaturated Al^{3+} ions on $\gamma\text{-Al}_2\text{O}_3$ act as binding centers to maintain the high dispersion of Pt atoms, but Pt rafts form as the loading amount of Pt increases (3). Currently, two major challenges remain in the field of atomically dispersed catalysts: (i) to ensure a loading content high enough for practical applications while maintaining the metal centers as individual sites under catalytic conditions (27, 28), and (ii) to address whether atomically dispersed catalysts offer distinct active sites and/or undergo catalytic pathways different from those of conventional metal catalysts (1, 4–6, 8–10, 12, 16–21).

We report a room-temperature photochemical strategy to fabricate a highly stable, atomically dispersed Pd catalyst (Pd_1/TiO_2) on ultrathin TiO_2 nanosheets with Pd loading up to 1.5%.

¹State Key Laboratory for Physical Chemistry of Solid Surfaces, Collaborative Innovation Center of Chemistry for Energy Materials, Engineering Research Center for Nano-Preparation Technology of Fujian Province, National Engineering Laboratory for Green Chemical Productions of Alcohols, Ethers, and Esters, and Department of Chemistry, College of Chemistry and Chemical Engineering, Xiamen University, Xiamen 361005, China. ²Institute of Physics, Chinese Academy of Sciences, Beijing 100190, China. ³Department of Chemistry, Dalhousie University, Halifax, Nova Scotia B3H 4R2, Canada.

*Corresponding author. Email: nfhzheng@xmu.edu.cn (N.Z.);



Large optical nonlinearity of indium tin oxide in its epsilon-near-zero region

M. Zahirul Alam, Israel De Leon and Robert W. Boyd (April 28, 2016)

Science **352** (6287), 795-797. [doi: 10.1126/science.aae0330]
originally published online April 28, 2016

Editor's Summary

Nonlinear optics: A surprise in store?

At ultrafast data rates, the ability to use light to control things could speed information processing. However, photons tend not to interact with each other, and so a nonlinear optical material is needed and the response of such materials is typically weak. Alam *et al.* report a surprising finding: that indium tin oxide, a commercially available transparent conducting oxide widely used in microelectronics, exhibits a large nonlinear response. They used a wavelength regime where the permittivity of the material is close to zero and observed a large and fast nonlinear optical response. The finding offers the possibility that other, so far unexplored, materials may be out there for nonlinear optical applications.

Science, this issue p. 795

This copy is for your personal, non-commercial use only.

Article Tools Visit the online version of this article to access the personalization and article tools:
<http://science.sciencemag.org/content/352/6287/795>

Permissions Obtain information about reproducing this article:
<http://www.sciencemag.org/about/permissions.dtl>

Science (print ISSN 0036-8075; online ISSN 1095-9203) is published weekly, except the last week in December, by the American Association for the Advancement of Science, 1200 New York Avenue NW, Washington, DC 20005. Copyright 2016 by the American Association for the Advancement of Science; all rights reserved. The title *Science* is a registered trademark of AAAS.



Supplementary Materials for
**Large optical nonlinearity of indium tin oxide
in its epsilon-near-zero region**

M. Zahirul Alam, Israel De Leon,* Robert W. Boyd

*Corresponding author. Email: ideleon@itesm.mx

Published 28 April 2016 on *Science* First Release
DOI: 10.1126/science.aae0330

This PDF file includes:

Materials and Methods
Supplementary Text
Figs. S1 to S4
References

Materials and Methods

Linear response of ITO

Our sample is a commercially available ITO film with sheet resistance of $\sim 5 \Omega/\text{square}$, deposited on a float glass substrate. The thickness of the film is $310 \pm 2 \text{ nm}$, and that of the substrate is 1.1 mm (Fig. 1A). The linear relative permittivity of the ITO film, ϵ , was measured via spectroscopic ellipsometry (Fig. 1B). Note that due to the large doping concentration, the optical properties of ITO at near-infrared wavelengths resemble those of a free electron gas. This is apparent from the excellent agreement between the experimental data (symbols) and the Drude model (solid curves), $\epsilon = \epsilon_\infty - \omega_p^2/(\omega^2 + i\gamma\omega)$ using a high-frequency permittivity of $\epsilon_\infty = 3.8055$, a damping rate of $\gamma = 0.0468\omega_p$, and a free-electron plasma frequency of $\omega_p/2\pi = 473 \text{ THz}$. The zero-permittivity condition, $\text{Re}(\epsilon)=0$, occurs at the bulk plasmon wavelength $\lambda_0 = 2\pi c\sqrt{\epsilon_\infty}/\omega_p = 1240 \text{ nm}$. At this wavelength the permittivity also has a large imaginary part, $\text{Im}(\epsilon) \approx 0.35$, associated with damping losses in the material.

Z-scan procedure

The z-scan technique (14) was used to study the intensity-dependent refractive index of the ITO film. In this technique, the sample is exposed to different optical intensities by translating it along the optical axis of the focused laser beam, and changes in the optical phase and attenuation of the transmitted light are measured as functions of the optical intensity. The measurements are taken over a broad spectral range covering the low permittivity region of the material and with a broad range of angles of incidence. The recorded data is then used to extract the effective nonlinear refractive index, $n_{2(\text{eff})}$, and the effective nonlinear attenuation constant, $\beta_{(\text{eff})}$. These parameters are defined as $n_{2(\text{eff})} = \Delta n/I$ and $\beta_{(\text{eff})} = \Delta\alpha/I$, where Δn and $\Delta\alpha$ are, respectively, the change in refractive index and the change in attenuation constant induced by the laser beam, and I is the intensity of the beam at its focus. For all our z-scan measurements, we used a pulsed laser (150 fs pulse duration, repetition rate of 1 kHz) with average incident power of $60 \mu\text{W}$ across the spectrum. This average power corresponds to a peak intensity of 66 GW/cm^2 at the beam's focus at a wavelength of 1240 nm.

We used a pinhole of 0.3 mm diameter to produce a beam with circularly symmetric trimmed Airy profile in the far-field. A series of lenses was then used to collimate and enlarge the beam. Part of the collimated beam was routed to a reference photodiode to monitor power fluctuations. The rest of the collimated beam was then focused onto the sample using an achromatic doublet lens with anti-reflection coating. The focused spot size was $25 \mu\text{m}$. The diffracted light after the sample was split using a pellicle beam splitter and routed to a pair of detectors for closed and open aperture measurements. The sample was mounted on a computer-controlled motorized translation stage. For each position of the sample we record the truncated mean values (the lowest 25% and the highest 25% values were discarded before calculating the mean) from the photodiodes averaged over roughly 3000 pulses. The signals from both closed- and open-aperture photodiodes were normalized by the signal obtained from the reference photodiodes to minimize the noise induced by the fluctuation of the laser beam intensity.

We used the Fresnel-Kirchhoff diffraction integral using a fast-Fourier-transform-based beam propagation method to simulate the experimental beam propagation over the entire setup, and the z-dependence of the signal at the closed-aperture and open aperture photodiodes (23). We have not made any *a priori* assumptions about the magnitude of the nonlinear phase shift. It is critical to our experiment that we not make such an assumption because the total nonlinear phase shift was quite large, which may invalidate the standard closed-form expressions for the far-field z-scan signals (14). We performed numerical simulations of the nonlinear setup to determine the z-dependence of the open- and closed-aperture signals. We verified our calculations by reproducing the results of other authors for both small and large phase shifts (14, 24). The shape of the closed-aperture signal is dependent on the shape of the open-aperture. Hence it is necessary to first extract the imaginary part of the phase shift. In order to extract the value of the phase shifts (real and imaginary) we followed the following steps. First, we generated a wavelength and angle dependent grid containing nonlinear imaginary phase shifts (step size of 0.0002 rad) and the maximum normalized net increase in transmittance at the open aperture photodiode. Then, for each value of the imaginary phase shift we produced corresponding wavelength and angle dependent grid containing nonlinear real phase shifts (step size of 0.0002 rad) and the transmission separation between the peak and the valley. We used the first grid to find the imaginary part of the phase shift from the open aperture data and the later grid to find the acquired real part of the phase shift. The extracted values of the nonlinear phase were used in the standard expression to calculate $n_{2(\text{eff})}$ and $\beta_{(\text{eff})}$ (17). Fig. S1 shows representative close- and open-aperture measurements at $\lambda = 1240$ nm.

Extraction of refractive index from transmittance and reflectance measurements

We estimated the effective complex refractive index of the ITO film associated with each set of transmittance and reflectance measurements for a given incident intensity. We use a nonlinear constrained optimization technique to find the simultaneous minima of the reflectance and the transmittance functions obtained using a linear transfer-matrix method. In our calculations we assumed that the refractive index of the substrate is independent of the intensity and took the substrate (glass) as an incoherent layer. This assumption is justified because the nonlinear optical response of the substrate is orders of magnitude weaker than that of the ITO film. We solve the minimization problem using the Nelder-Mead method. For each iteration of simultaneous minima finding operation we used the linear complex refractive index as the initial guess.

Pump-probe response

We measured the transmittance of a weak probe as a function of the delay between the probe and a strong pump of the same wavelength. The transient change in the optical properties of ITO is proportional to the transient change in the temperature of the electrons. Hence, the transmittance of the probe for a particular pump-probe delay is proportional to the convolution of the temporal response of the hot electrons with the probe pulse. In a typical pump-probe measurement, it is often necessary to use lock-in detection techniques. However, in our experiment the change in transmittance of the probe is so strong that we did not require any such sensitivity-enhancement techniques. We have observed that the overall response time has a minor frequency dependence: the system relaxes more quickly when pumped with a shorter wavelength. This variation is

due simply to the fact that higher photon energy leads to faster relaxation of electron to the Fermi level because $\tau_{ee} \propto (h\nu)^{-1}$.

Supplementary Text

Two-temperature model

The free-electron dynamics in ITO are metal-like and can be described by the Drude model. Hence, we assume that the third-order self-action nonlinear response of ITO in the ENZ regime is dominated by the response of the free-electrons. To describe this nonlinear mechanism, we use a phenomenological two-temperature model (18). This model has been successfully applied by many authors to explain the ultrafast nonlinear response of metals irradiated by femtosecond pulses (18, 20, 21, 25). According to the two-temperature model, the laser energy absorbed by the material is transferred to non-thermalized electrons (known as “hot electrons”) by promoting some free-electrons lying below the Fermi level to the unoccupied levels above the Fermi level.

The self-action nonlinear process due to the hot-electron dynamics has a finite response time, i.e. the maximum response is delayed with respect to the peak of the laser excitation. In noble metals the total relaxation time of the hot electrons is a few picoseconds and is limited by the electron-phonon interaction time. However the response of the ITO thin film deviates from that of the metal in three important ways: *i*) unlike noble metals, ITO has no interband transition resonance in the visible or infrared range of the optical spectrum; *ii*) the free-electron density in ITO is two orders of magnitude smaller than that of noble metals such as gold, resulting in much smaller electron heat capacity and larger change in the electron temperature if all other parameters are held constant; and *iii*) owing to a relatively smaller free-electron density, the Fermi level is quite low in the conduction band (~ 1 eV for ITO). Due to the last property, infrared radiation at ENZ wavelengths can excite even the lowest-energy conduction band electrons (in contrast, the Fermi level of gold is ~ 6.42 eV and IR light only excite only those electrons that sits near the Fermi level).

According to the delayed two-temperature model, after the laser pulse is absorbed the generated hot electrons acquire a non-thermal energy distribution and act as a delayed source of heating. The overall dynamics of the conduction band electrons can be described by the following system of phenomenological coupled differential equations (25) :

$$C_e \frac{\partial T_e}{\partial t} = -g_{ep}(T_e - T_l) + \frac{N}{2\tau_{ee}}, \#(S1A)$$

$$C_l \frac{\partial T_l}{\partial t} = g_{ep}(T_e - T_l) + \frac{N}{2\tau_{ep}}, \#(S1B)\#$$

$$\frac{\partial N}{\partial t} = -\frac{N}{2\tau_{ee}} - \frac{N}{2\tau_{ep}} + P, \#(S1C)$$

Here, N is the non-thermal energy density stored in the excited electrons, g_{ep} is the electron-phonon coupling coefficient, T_e (T_l) is the free-electron (lattice) temperature, C_e (C_l) is the heat capacity of the electrons (lattice), τ_{ee} (τ_{ep}) is the electron-electron (electron-phonon) relaxation time, and P is the time dependent absorbed power density (i.e., rate of energy density absorbed in the material). We have ignored thermal diffusion

processes in Eq. (S1). In the transverse dimension the beam size greatly exceeds the electrons thermal diffusion length and hence we also ignore the transverse dependence. We have also ignored the thermal diffusion in the longitudinal direction by assuming constant absorbed energy density.

In general, the thermal diffusivity of the electrons is a function of the electron temperature and the velocity. Since the hot electrons in a noble metal move approximately at the Fermi velocity, the heat transport is ballistic within the momentum relaxation length due to electron-electron interaction. Heat is transported much faster by the electrons than through the lattice, and hence typically the lattice contribution to the thermal diffusion can be ignored (19). We also ignored the heat diffusion by hot electrons in transverse dimension. The heat diffusion length is much shorter than the spot size and hence it can be safely ignored.

Next we estimate the different parameters for ITO that appear in Eqs. (S1). The electron-phonon coupling coefficient (g_{ep}) determines the strength of the energy exchange between the excited electrons and the vibrational modes of the lattice. We estimate this parameter as

$$g_{ep} = 0.562n_e \frac{k_B^2 \Theta_D^2 v_F}{L_f T_l E_F}, \#(S2)$$

where k_B is Boltzmann's constant, L_f is the electron mean free path, v_F and E_F are the Fermi velocity and the Fermi energy respectively, Θ_D is the Debye temperature, and n_e is the free-electron density.

The electron-electron (τ_{ee}) and electron-phonon (τ_{ep}) relaxation times in Eqs. (S1) dictate the rate at which the absorbed energy is redistributed to the electrons and to the lattice respectively. These quantities are given by (26, 27)

$$\tau_{ee} = C \left\{ \frac{\omega^2}{4\pi^2 \omega_p} \left[1 + \left(\frac{2\pi k_B T_e}{\hbar \omega} \right)^2 \right] \right\}^{-1}, \#(S3A)$$

$$\tau_{ep} = 2 \frac{C_e}{g_{ep}}, \#(S3B)$$

where ω_p is the free-electron plasma frequency and ω is the frequency of the laser beam. Here, we use the parameter C in Eq. (S3A) as a scaling factor to make sure that the Drude damping parameter, γ , measured under thermal equilibrium (at a temperature of 300 K) is equal to $1/\tau_{ep} + 1/\tau_{ee}$.

The free-electron heat capacity (C_e) is a function of temperature. For temperatures smaller than the Fermi temperature, this quantity can be approximated as $C_e = 3 \pi^2 n_e k_B T_e / \sqrt{36 T_F^2 + 4\pi^4 T_e^2}$. On the other hand, the lattice heat capacity (C_l) depends on Θ_D . The value of Θ_D for ITO nanostructures is reported (28) to be ~ 1000 K, which is much larger than that of noble metals such as gold (~ 170 K). The Debye temperature Θ_D is defined as the temperature required for the excitation of the highest-frequency phonon mode - and thus, for the excitation all phonon modes. Hence, for lattice temperatures much lower than Θ_D , the number of the interacting phonon modes and, by extension, the lattice heat capacity (C_l) is a strong function of the lattice temperature. However, the lattice heat capacity asymptotically approaches a constant value as the lattice temperature approaches Θ_D . Therefore, even for $T_l \approx \Theta_D/2$, the temperature dependent variation is

small. Hence, we ignore this variation and find that a constant lattice heat capacity of $2.6 \times 10^6 \text{ Jm}^{-3}\text{K}^{-1}$ (which is slightly larger than the heat capacity of In_2O_3) can reproduce our experimental results.

Finally, the absorbed power density (P) is given by

$$P(t) = (1 - R - T)I_0\alpha \exp\left[-2\left(\frac{t}{\tau_p}\right)^2\right], \#(S4)$$

where R , T and α are the wavelength dependent reflectance, transmittance and absorption coefficient, respectively, and τ_p is the laser pulse duration. In general, $P(t)$ is also spatially varying because of absorption within the ITO sample. However, we ignore this variation by assuming an effective intensity, I_0 , that is constant over one absorption length.

Field enhancement at oblique incidence

According to Maxwell's equations, the longitudinal component of the displacement field must be continuous across an interface. Thus, the longitudinal component of the electric field inside ITO is inversely proportional to the permittivity of ITO. For instance, for the case of a single ITO-air interface, this continuity condition yields the following relation for the field components normal to the interface: $E_{\perp, \text{ITO}} = E_{\perp, \text{air}}/\epsilon_{\text{ITO}}$. Thus, for obliquely incident TM polarized light, the field inside the ITO is enhanced when ϵ_{ITO} is small. This enhancement, however, is limited by the non-vanishing imaginary part of the dielectric constant. We calculated the field enhancement factor as a function of wavelength and angle of incidence for TM polarized light using a transfer-matrix method and the measured linear permittivity values of our ITO sample. We show the result in Fig. S2.

Hot-electron-induced change of refractive index

A change in the electron temperature produces a change in complex refractive index of the material. The electron dynamics under non-equilibrium conditions and the associated change in the refractive index are complex many-body problems that require detailed knowledge of the electronic band structure. Since we lack this knowledge, it is difficult to model the non-equilibrium electronic dynamics from an *ab initio* approach. Therefore, we use a phenomenological approach based on the two-temperature model and the Drude model to describe the hot-electron induced change in refractive index.

The two-temperature model predicts a transient but large change in the electronic temperature, which results in a significant modification of the Fermi-Dirac distribution and a corresponding decrease in the free electron polarizability (29). Within the framework of the Drude model, this decrease in the polarizability is equivalent to a red-shift of the plasma frequency due to the temperature dependence of the Fermi level (17). This view is consistent with that of other authors who have investigated the nonlinear transient response of metal-ITO hybrid structures (2). Because of the complex physical mechanism relating the change in refractive index, Δn , to the change in free-electron temperature, ΔT_e , the relationship between these two quantities is not linear. This conclusion is also supported by the relationship between T_e and the electron-electron scattering rate (τ_{ee}^{-1}). At ENZ frequencies the photon energy ($h\nu$) is approximately equal to the Fermi energy (ϵ_F) of the conduction band electrons, and thus τ_{ee}^{-1} , the dominant dephasing mechanism, is a quadratic function of the electronic temperature ($\tau_{ee}^{-1} \propto T_e^2$)

(26, 30, 31). A change in the scattering rate results in the modification of the damping term in the Drude model. Since the change in the real and imaginary parts of the permittivity is related by the Kramers-Kronig relation, the relationship between ΔT_e and Δn is nonlinear.

The electron-electron scattering process distributes the absorbed energy among the electrons, and a short time after the passing of the pulse produces a hot Fermi distribution with electron temperature T_e (assuming that the total internal energy is constant). At this stage, electrons are in equilibrium with each other; however, they are not in equilibrium with the lattice. For a given electron density, the chemical potential (Fermi level) of a metal-like material depends on the temperature of the free electrons. Thus a change in the electron temperature produces a change of the chemical potential. Finally, the hot-electrons comes to the thermal equilibrium with the lattice through electron-phonon interaction. This results in an increase in the lattice temperature. The lattice energy is dissipated to the environment at a much longer time scale. However, low repetition rate of the laser ensures that the lattice is always at the thermal equilibrium with the laboratory before the arrival of an optical pulse.

The electronic temperature-dependent chemical potential (or Fermi level), $\mu(T_e)$, is related to the Fermi energy by (32)

$$\mu(T_e) \approx \varepsilon_F \left[1 - \frac{\pi^2}{12} \left(\frac{T_e}{T_F} \right)^2 \right], \#(S5)$$

where T_F is the Fermi temperature. This relation allows one to estimate the effective plasma frequency at the elevated electronic temperature (for $T_e \ll T_F$.) and then use the Drude-Sommerfeld model of metals to calculate the change in the refractive index, Δn .

Using this method to calculate Δn , we obtained the enhancement of $n_{2(\text{eff})} = \Delta n/I$ as a function of the wavelength and the angle of incidence. This enhancement, shown in Fig. S3, is defined with respect to the value obtained at normal incidence at a wavelength $\lambda = 970$ nm. Note that for this calculation we have taken into account the wavelength and angle dependent field enhancement factor shown in Fig. S2. Our calculation is correct within the first order approximation, and shows that a modest field enhancement can result in significant enhancement of $n_{2(\text{eff})}$.

Effect of the non-linear change of reflectivity

In their seminal paper proposing the z-scan technique, Sheik-Bahae *et al.* (13) ignored the change in the Fresnel reflectivity due to the nonlinear optical effects. This approximation neglects any change in the internal optical intensity that may result from an optically induced increase or reduction of the Fresnel reflection. This approximation is excellent for most materials, including those exhibiting large nonlinear refractive index coefficients, because the nonlinear change in the refractive index, Δn , is typically much smaller than the linear refractive index, n . However, this is not the case for the experimental situation that we present in the main text, where Δn is similar to or even larger than n . As a concrete example, consider the results in Fig. 3a of the main text, where we show that the reflectance at $\theta = 30^\circ$ can change from a value of $R_L = 0.187$ for the linear case, to a value of $R_{NL} = 0.032$ for the most extreme nonlinear case – i.e., when the nonlinear response saturates. For the z-scan analysis in the main text, we always estimated the intensity within the sample by accounting for the Fresnel reflection using the value of the linear reflectance, i.e., $I = I_0(1 - R_L)$, where I_0 is the intensity of the beam

at its focus and I is the intensity within the sample. However, as we explain next, this approximation leads to inaccuracies when extracting the values of $n_{2(\text{eff})}$ and $\beta_{(\text{eff})}$.

The maximum changes in the input laser intensities in the z -scan measurements are related to the maximum changes in the Fresnel reflectivities due to the nonlinear response of ITO. Since $T + A = 1 - R$, a nonlinear change in reflectance (R) necessarily implies changes in nonlinear absorptance (A) and transmittance (T) due to the increase in input intensities. Thus, a nonlinear change in reflectance affects both open and closed-aperture measurements. However, we ignore the effect of the nonlinear Fresnel reflectivity in our calculation. Hence, there are uncertainties in the extracted values of $n_{2(\text{eff})}$ and $\beta_{(\text{eff})}$. The saturated values of the reflectance determine the maximum possible nonlinear changes in the input intensities. We estimate the upper bound to fractional error in the extracted nonlinear coefficients as

$$\zeta_{(\text{max})} = 1 - \frac{1-R_L}{1-R_{\text{NL}(\text{sat})}}, \#(S6)$$

where $R_{\text{NL}(\text{sat})}$ is the reflectance of the sample in the high intensity limit in which the change in refractive index reaches its maximum (saturated) value. The subscript L indicates linear value. For the particular case discussed above ($\theta = 30^\circ$), this maximum error is 19%. However, this error is not constant for all θ because the reflectance varies with θ . To estimate the maximum error for all the angles of incidence used in our experiments, we calculated $R_{\text{NL}(\text{sat})}$ as a function of θ taking the saturated refractive index value of the ITO film, i.e., $n_{(\text{sat})} = 1.13 + i0.27$. This is a safe assumption, since we expect the saturated value of Δn to be the same regardless of the incident angle. We use this value in Eq. (S6) to obtain the maximum error expected in the extracted values of the nonlinear coefficients, which occurs when the input intensity is large enough to saturate the nonlinear optical response of the material. These calculated maximum errors are shown in Fig. S4.

Practical uses of the optical nonlinearity of ITO

ITO is a lossy material at ENZ frequencies. The losses in this material are significantly larger than those in other highly nonlinear materials, such as chalcogenide glass. For instance, the linear absorption coefficient of our ITO sample is roughly $4.2 \mu\text{m}^{-1}$ at $\lambda = 1240 \text{ nm}$. Given the nature of its optical nonlinearity, ITO is probably not suitable to construct nonlinear devices requiring long propagation lengths. Rather, the large refractive index change accessible with ITO could be used in conjunction with nanoplasmonics and nanophotonics (where propagation lengths are very short) to create efficient nanoscopic nonlinear devices. For instance, the large change of refractive index of ITO can be extremely useful when combined with plasmonic nanostructures, whose optical properties are extremely sensitive to the refractive index around them. Moreover, the ultrafast recovery time and large change in absorption may allow one to use a thin film of ITO at ENZ wavelengths as a saturable absorber in a mode-locked laser.

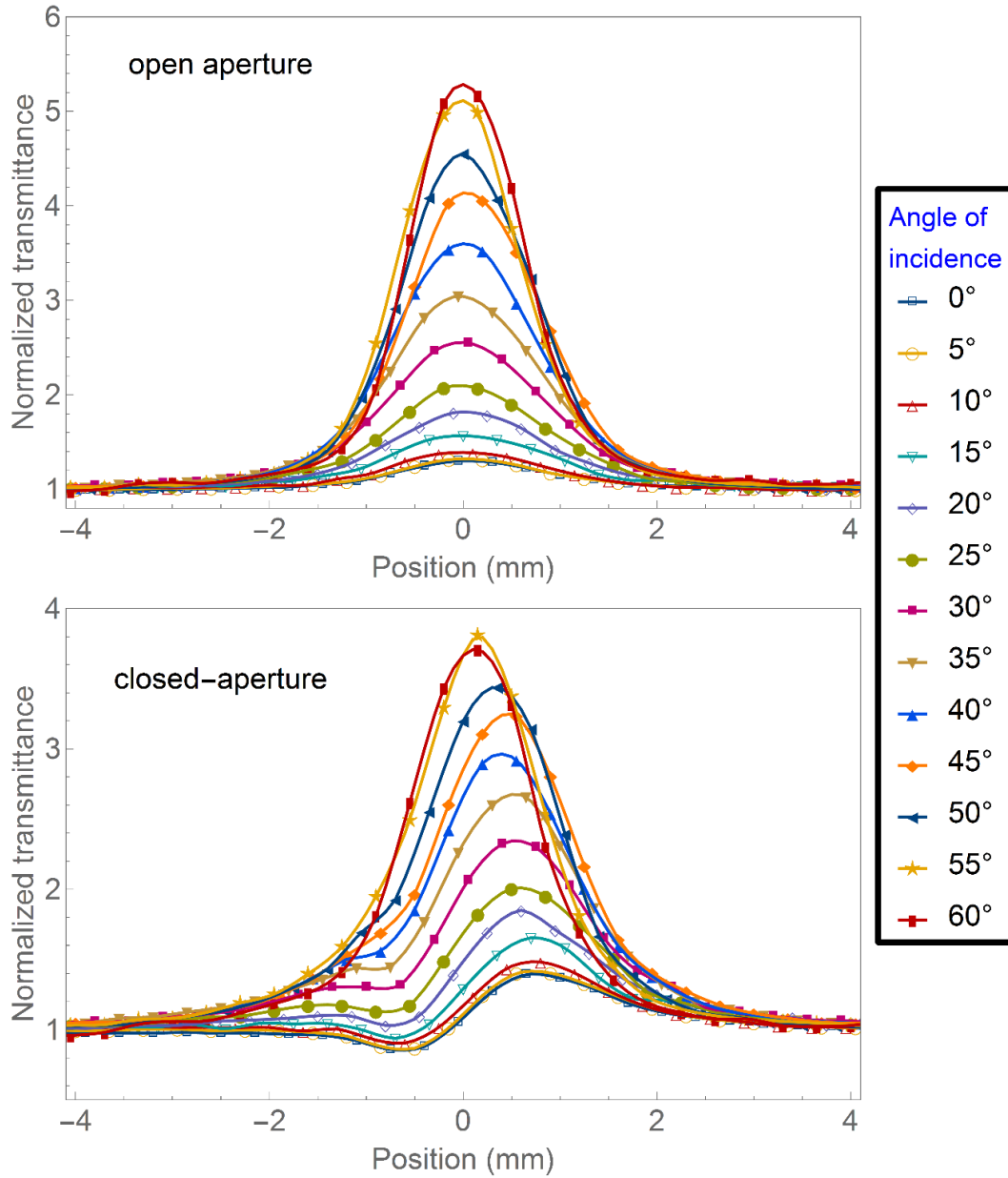


Fig. S1.

Open- and closed-aperture measurements at $\lambda = 1240$ nm for various angles of incidence. The asymmetry in the closed-aperture signal increases with increasing angle of incidence due to the large change in the absorption.

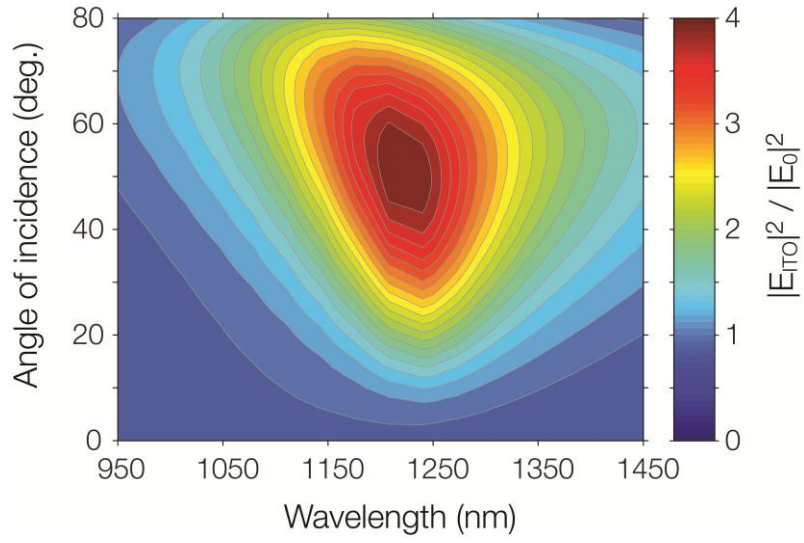


Fig. S2

Field enhancement at the air-ITO interface for obliquely incident TM polarized light. The maximum field enhancement factor is 4, and occurs at wavelengths around $\lambda_0 = 1240$ nm.

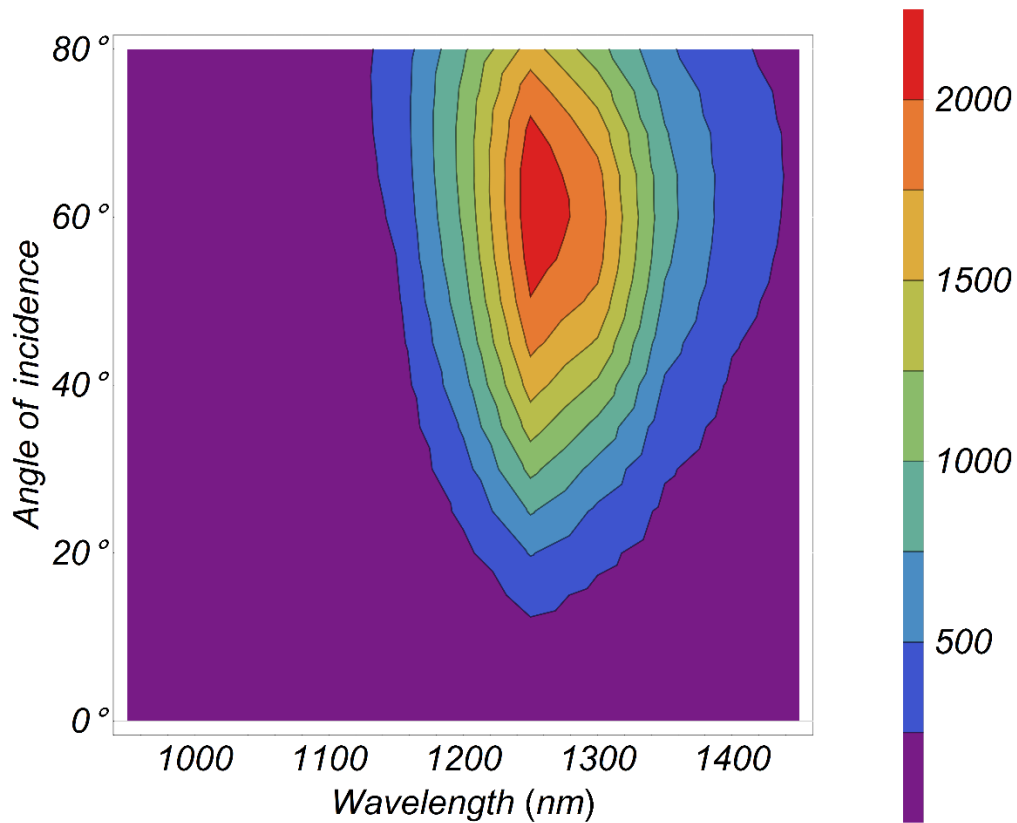


Fig. S3.

Enhancement of $n_{2(\text{eff})}$ calculated using a first-order approximation to the electronic temperature-dependent red-shift of the plasma frequency. We used the $n_{2(\text{eff})}$ value at $\lambda = 970$ nm as the normalization factor. For this calculation we have used an incident intensity of 20 GW/cm^2 .

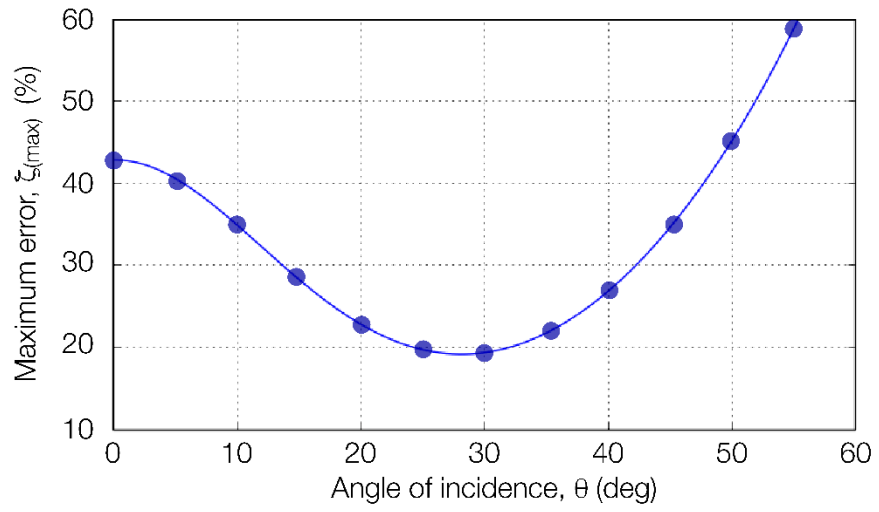


Fig. S4.

Maximum error in the extracted nonlinear coefficients when the input intensity is large enough to saturate the nonlinear optical response of the material. The values plotted here were calculated using Eq.(S6).

References

1. M. Kauranen, A. V. Zayats, Nonlinear plasmonics. *Nat. Photonics* **6**, 737–748 (2012). [doi:10.1038/nphoton.2012.244](https://doi.org/10.1038/nphoton.2012.244)
2. M. Abb, P. Albella, J. Aizpurua, O. L. Muskens, All-optical control of a single plasmonic nanoantenna-ITO hybrid. *Nano Lett.* **11**, 2457–2463 (2011). [Medline doi:10.1021/nl200901w](https://doi.org/10.1021/nl200901w)
3. A. D. Neira, N. Olivier, M. E. Nasir, W. Dickson, G. A. Wurtz, A. V. Zayats, Eliminating material constraints for nonlinearity with plasmonic metamaterials. *Nat. Commun.* **6**, 7757 (2015). [Medline doi:10.1038/ncomms8757](https://doi.org/10.1038/ncomms8757)
4. M. Silveirinha, N. Engheta, Tunneling of electromagnetic energy through subwavelength channels and bends using ϵ -near-zero materials. *Phys. Rev. Lett.* **97**, 157403 (2006). [Medline doi:10.1103/PhysRevLett.97.157403](https://doi.org/10.1103/PhysRevLett.97.157403)
5. A. Alù, M. Silveirinha, A. Salandrino, N. Engheta, Epsilon-near-zero metamaterials and electromagnetic sources: Tailoring the radiation phase pattern. *Phys. Rev. B* **75**, 155410 (2007). [doi:10.1103/PhysRevB.75.155410](https://doi.org/10.1103/PhysRevB.75.155410)
6. A. R. Davoyan, A. M. Mahmoud, N. Engheta, Optical isolation with epsilon-near-zero metamaterials. *Opt. Express* **21**, 3279–3286 (2013). [Medline doi:10.1364/OE.21.003279](https://doi.org/10.1364/OE.21.003279)
7. H. Suchowski, K. O'Brien, Z. J. Wong, A. Salandrino, X. Yin, X. Zhang, Phase mismatch-free nonlinear propagation in optical zero-index materials. *Science* **342**, 1223–1226 (2013). [Medline doi:10.1126/science.1244303](https://doi.org/10.1126/science.1244303)
8. A. Capretti, Y. Wang, N. Engheta, L. Dal Negro, Enhanced third-harmonic generation in Si-compatible epsilon-near-zero indium tin oxide nanolayers. *Opt. Lett.* **40**, 1500–1503 (2015). [Medline doi:10.1364/OL.40.001500](https://doi.org/10.1364/OL.40.001500)
9. T. S. Luk, D. de Ceglia, S. Liu, G. A. Keeler, R. P. Prasankumar, M. A. Vincenti, M. Scalora, M. B. Sinclair, S. Campione, Enhanced third harmonic generation from the epsilon-near-zero modes of ultrathin films. *Appl. Phys. Lett.* **106**, 151103 (2015). [doi:10.1063/1.4917457](https://doi.org/10.1063/1.4917457)
10. N. Kinsey, C. DeVault, J. Kim, M. Ferrera, V. M. Shalaev, A. Boltasseva, Epsilon-near-zero Al-doped ZnO for ultrafast switching at telecom wavelengths. *Optica* **2**, 616 (2015). [doi:10.1364/OPTICA.2.000616](https://doi.org/10.1364/OPTICA.2.000616)
11. G. V. Naik, V. M. Shalaev, A. Boltasseva, Alternative plasmonic materials: Beyond gold and silver. *Adv. Mater.* **25**, 3264–3294 (2013). [Medline doi:10.1002/adma.201205076](https://doi.org/10.1002/adma.201205076)
12. E. Feigenbaum, K. Diest, H. A. Atwater, Unity-order index change in transparent conducting oxides at visible frequencies. *Nano Lett.* **10**, 2111–2116 (2010). [Medline doi:10.1021/nl1006307](https://doi.org/10.1021/nl1006307)
13. M. Sheik-Bahae, A. A. Said, T.-H. Wei, D. J. Hagan, E. W. Van Stryland, Sensitive measurement of optical nonlinearities using a single beam. *IEEE J. Quantum Electron.* **26**, 760–769 (1990). [doi:10.1109/3.53394](https://doi.org/10.1109/3.53394)
14. B. K. Rhee, J. S. Byun, E. W. Van Stryland, Z scan using circularly symmetric beams. *J. Opt. Soc. Am. B* **13**, 2720 (1996). [doi:10.1364/JOSAB.13.002720](https://doi.org/10.1364/JOSAB.13.002720)
15. H. I. Elim, W. Ji, F. Zhu, Carrier concentration dependence of optical Kerr nonlinearity in indium tin oxide films. *Appl. Phys. B* **82**, 439–442 (2006). [doi:10.1007/s00340-005-2079-8](https://doi.org/10.1007/s00340-005-2079-8)

16. See supplementary materials on *Science Online*.

17. R. W. Boyd, *Nonlinear Optics* (Elsevier, 2008).

18. C. Sun, F. Vallée, L. Acioli, E. P. Ippen, J. G. Fujimoto, Femtosecond investigation of electron thermalization in gold. *Phys. Rev. B Condens. Matter* **48**, 12365–12368 (1993). [Medline](#)
[doi:10.1103/PhysRevB.48.12365](https://doi.org/10.1103/PhysRevB.48.12365)

19. S. D. Brorson, J. G. Fujimoto, E. P. Ippen, Femtosecond electronic heat-transport dynamics in thin gold films. *Phys. Rev. Lett.* **59**, 1962–1965 (1987). [Medline](#)
[doi:10.1103/PhysRevLett.59.1962](https://doi.org/10.1103/PhysRevLett.59.1962)

20. E. Carpena, Ultrafast laser irradiation of metals: Beyond the two-temperature model. *Phys. Rev. B* **74**, 024301 (2006). [doi:10.1103/PhysRevB.74.024301](https://doi.org/10.1103/PhysRevB.74.024301)

21. B. Rethfeld, A. Kaiser, M. Vicanek, G. Simon, Ultrafast dynamics of nonequilibrium electrons in metals under femtosecond laser irradiation. *Phys. Rev. B* **65**, 214303 (2002).
[doi:10.1103/PhysRevB.65.214303](https://doi.org/10.1103/PhysRevB.65.214303)

22. D. de Ceglia, S. Campione, M. A. Vincenti, F. Capolino, M. Scalora, Low-damping epsilon-near-zero slabs: Nonlinear and nonlocal optical properties. *Phys. Rev. B* **87**, 155140 (2013).
[doi:10.1103/PhysRevB.87.155140](https://doi.org/10.1103/PhysRevB.87.155140)

23. B. Yao, L. Ren, X. Hou, Z-scan theory based on a diffraction model. *J. Opt. Soc. Am. B* **20**, 1290 (2003). [doi:10.1364/JOSAB.20.001290](https://doi.org/10.1364/JOSAB.20.001290)

24. C. Kwak, Y. Lee, S. Kim, Analysis of asymmetric Z-scan measurement for large optical nonlinearities in an amorphous As₂S₃ thin film. *J. Opt. Soc. Am. B* **16**, 600–604 (1999).
[doi:10.1364/JOSAB.16.000600](https://doi.org/10.1364/JOSAB.16.000600)

25. M. Conforti, G. Della Valle, Derivation of third-order nonlinear susceptibility of thin metal films as a delayed optical response. *Phys. Rev. B* **85**, 245423 (2012).
[doi:10.1103/PhysRevB.85.245423](https://doi.org/10.1103/PhysRevB.85.245423)

26. N. Del Fatti, C. Voisin, M. Achermann, S. Tzortzakis, D. Christofilos, F. Vallée, Nonequilibrium electron dynamics in noble metals. *Phys. Rev. B* **61**, 16956–16966 (2000).
[doi:10.1103/PhysRevB.61.16956](https://doi.org/10.1103/PhysRevB.61.16956)

27. C. Voisin, N. Del Fatti, D. Christofilos, F. Vallée, Ultrafast electron dynamics and optical nonlinearities in metal nanoparticles. *J. Phys. Chem. B* **105**, 2264–2280 (2001).
[doi:10.1021/jp0038153](https://doi.org/10.1021/jp0038153)

28. J. J. Lin, Z. Q. Li, Electronic conduction properties of indium tin oxide: Single-particle and many-body transport. *J. Phys. Condens. Matter* **26**, 343201 (2014). [Medline](#)
[doi:10.1088/0953-8984/26/34/343201](https://doi.org/10.1088/0953-8984/26/34/343201)

29. D. Pines, *Elementary Excitations in Solids: Lectures on Phonons, Electrons, and Plasmons* (Advanced Book Classics, 1966).

30. F. Ladstädter, U. Hohenester, P. Puschnig, C. Ambrosch-Draxl, First-principles calculation of hot-electron scattering in metals. *Phys. Rev. B* **70**, 235125 (2004).
[doi:10.1103/PhysRevB.70.235125](https://doi.org/10.1103/PhysRevB.70.235125)

31. M. Kaveh, N. Wiser, Electron-electron scattering in conducting materials. *Adv. Phys.* **33**, 257–372 (1984). [doi:10.1080/00018738400101671](https://doi.org/10.1080/00018738400101671)

32. N. W. Ashcroft, N. D. Mermin, *Solid State Physics* (Brooks Cole Publishing, 1976).